CLM-P648

UKAEA

Preprint

SOFT X-RAY INSTRUMENTATION FOR FUSION PLASMA STUDIES

N. J. PEACOCK

CULHAM LABORATORY
Abingdon Oxfordshire

1981

CLM-P 648

SOFT X-RAY INSTRUMENTATION FOR FUSION PLASMA STUDIES

N J Peacock
Culham Laboratory, Abingdon, Oxon, OX14 3DB, UK
(Euratom/UKAEA Fusion Association)

ABSTRACT

Both crystal dispersion and diffraction grating instruments are routinely ısed for soft X-ray dispersion in the fusion programme at the Culham Laboratory /here the keV plasmas studied range from highly transient, high density $n_e \gtrsim$ $.0^{21}$ cm^{-3}, laser-produced plasmas to relatively low density, $n_e \gtrsim 10^{13}$ cm^{-3} ;okamak plasmas. In this paper the soft X-ray spectral features from these ılasmas are discussed and the design parameters of appropriate instruments for :-ray studies are considered.

Useful spectral surveys of laser-produced plasmas have been obtained using rystals bent convex in the de Broglie mode; higher aperture concave Johann onfigurations have been designed and constructed with multichannel read out or tokamak studies. Grazing incidence diffraction grating instruments have een operated in the photographic survey mode and as double channel monochromators. perating experience with existing instruments is assessed. Examples of spectral nformation in the wavelength region $\sim$ 4 Å to $\sim$ 400 Å are presented and their use n plasma diagnostic studies is discussed.

(Submitted for publication in Journal of Applied Physics)

ıne 1981
EW/CMS

I. INTRODUCTION

Within the wide range of possible measurement
niques available to physicists in their studies of
temperature plasmas of thermonuclear fusion
erest [1] - [6] perhaps the most informative are
se diagnostics which operate in the soft X-ray
ion of the spectrum, hν ∿ 1 keV [7].

In 'state of the art' fusion experiments, electron
peratures $kT_e \gtrsim 1$ keV are commonly achieved both in
density, $n_e \simeq 10^{13} cm^{-3}$, magnetic confinement devices
as tokamaks and in inertially-confined plasmas
e liquid densities or above have been reached. The
tral intensity of the continuum emission, neglecting
the moment any recombination steps, will peak at
$_X$ = 2 kTe. Line emission from all ions which might
resent in the plasma, excepting the lightest gases,
extend throughout the VUV and soft X-ray regions;
as far as hν ∿ 10 kTe for some, hydrogen-like and
um-like ion configurations. Figure 1, for example,
strates the energy spread of the more intense
sion lines from iron. Most of the line features
quantum energies between 31 eV and 1.24 keV, ie,
Å and 10 Å. The approximate temperature at which the
will appear in ionisation equilibrium is the ap-
riate excitation energy for the Δn = 1 transitions

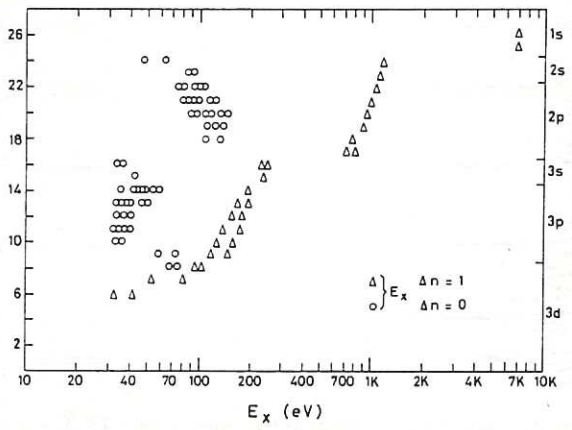

ig 1. Excitation energies E_x, of Δn = 1, Δn = 0
ransitions in Iron ions of charge state q.

divided by a factor between 1 and 4. At temperatures $\gtrsim$ 1 keV the most intense resonance Δn = 1 lines of the common metals lie in the X-ray region proper, see Figure 1; but, even in multi-keV plasmas, interest in the soft X-ray region and in the VUV region is sustained since the thermal energy X-ray lines and continuua can readily be confused with emission from a high energy tail of a distorted Maxwellian electron energy distribution. This is very nicely illustrated by the coded aperture images of laser irradiated microballoon targets [8], where the higher energy X-ray emission from supra thermal electrons at the surface of the irradiated shell can in this case be clearly distinguished from the softer, thermal emission from the compressed core plasma. The soft X-ray emission, ∿ 0.1 keV to ∿ 1 keV, remains, therefore, a more characteristic monitor of the bulk thermal content of the plasma.

The present paper sets out first of all to describe the plasma and atomic rate processes which give rise to these spectral features which are of prime diagnostic interest. Although tokamaks and laser-irradiated targets frequently generate the same ion species, these sources are discussed separately since their diagnostic requirements are usually very different. In tokamaks, for example, impurity ion diffusion might be the most important parameter to derive from soft X-ray spectroscopy, while in laser compression experiments line broadening leading to values of the compressed density, ρ gm cm^{-3} and of the inertial confinement factor, $\int \rho . dr$ gm cm^{-2}, are often the most sought after parameters.

The design criteria for X-ray instrumentation is discussed bearing in mind the possibility of investigating specific aspects of plasma behaviour. Stated in a different way, the instruments are designed with a particular diagnostic measurement in mind rather than as 'botanical' survey instruments for cataloguing spectral features. In section IV, we cite examples of the types of grazing-incidence grating spectrometers and crystal spectrometers that are in operation at the Culham Laboratory and we speculate on more ideal systems which require yet further development.

II SOFT X-RAY SPECTRAL FEATURES OF keV PLASMAS IN LABORATORY FUSION STUDIES

A. Tokamaks.

Tokamaks operating with plasmas whose electron temperature is typically kTe $\gtrsim$ 1 keV and with a central electron density in the range $5 \times 10^{12} \lesssim n_e \lesssim 5 \times 10^{14}$ cm^{-3}, have emission features in the soft X-ray region which are closely similar to those from solar active regions.

An electron temperature of $\sim$ 1 keV can be achieved almost routinely by simple ohmic heating. This value can, in principle, be increased by heating the electrons directly at the electron cyclotron resonance frequency, so-called ECRH heating. So far, with modest input powers of 0.1 MW, factors of two increase at sub keV temperatures have been achieved [9]. More indirectly, the electron heat content can also be increased, via the ions, by wave heating at the ion resonance frequencies [10]. Auxiliary heating with particle (eg H^0) beams is also topical [11] [12] and indirectly heats the electrons. At the multi-MW level in the PDX and PLT tokamaks [11] [12], particle beam heating has produced something of a record with ion temperatures as high as 7 keV and electron temperatures kTe $\sim$ 3 keV; these two temperatures are decoupled partly due to electron heat loss but mainly due to the low frequency of electron-ion collisions at $n_e \sim 1 \times 10^{13}$ cm^{-3}.

The main spectral features from these plasmas in the soft X-ray region are line emission from highly ionised impurities. Light elements eg O, N, C etc are present typically to the extent of 0.01 n_e, while heavier, usually metal impurities eg Ni Fe Ti Mo etc. from the walls and from current aperture limiters, have typical concentrations $\sim$ 0.001 n_e. In particularly clean tokamaks with gettering and divertors [13], these impurity concentrations can be reduced by an order of magnitude or more. We shall see section III, that this has an important bearing on instrument aperture for soft X-ray studies.

The metallic impurity ions in the core of a tokamak plasma have ionisation potentials, $\psi(q)$ where q is the ion charge state, which characteristically are three or four times the electron temperature and with the relative populations of the different charge states in approximately coronal equilibrium [14]. In the PLT tokamak at Princeton (PPL), however, the impurity ion species are located typically at somewhat higher values of Te on the Te(r) profile than would be predicted by coronal ionisation-recombination balance. Uncertainty in the atomic rate coefficients could account in some measure for the somewhat different conclusions of the TFR tokamak group [14] and of the Princeton Group. It appears that the spatial location of the ion populati is more sensitive to uncertainties in atomic rates than to possible variations in particle diffusion rat [15]. In the outer, lower temperature regions of the plasma, departures from coronal equilibrium are commonly observed due to the relatively rapid recycling the impurities between the plasma boundary and the limiter and vessel walls.

The low collision rates in tokamaks, $10^3 - 10^5$ s^{-1} ensures that forbidden lines which also appear in the solar spectrum and extend from the X-ray region to the visible are noteworthy features of the tokamak spectru Figure 2 illustrates the wavelength dependence of the forbidden and allowed lines from ions belonging to the carbon iso-electronic sequence. The allowed $\Delta n = 0$ transitions of the common metals lie in the extreme vacuum UV (XUV) region, 100 Å $\lesssim \lambda \lesssim$ 200 Å; the inter-system lines are at somewhat longer wavelengths while the important forbidden lines due to M1 transitions

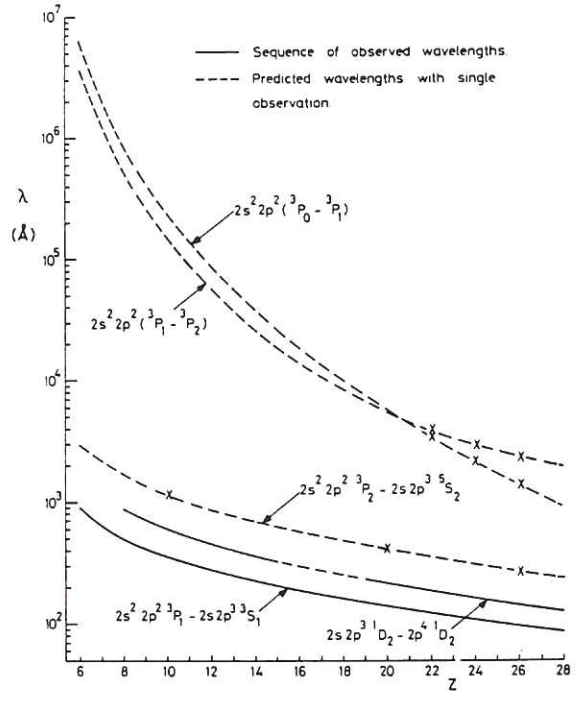

Fig 2. Wavelengths of some important transitions in carbon-like ions as a function of atomic number Z.

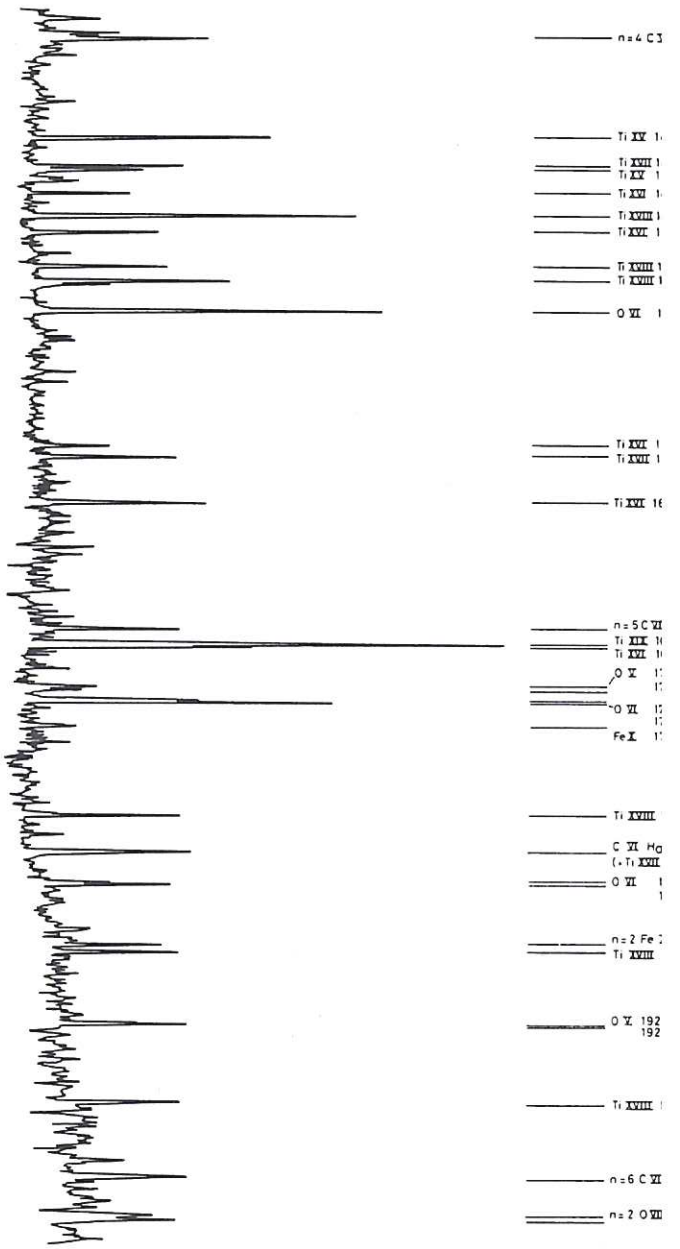

Fig 3. Section of soft X-ray spectrum (75 Å - 135 Å from DITE tokamak. The resonance lines of the light gas ions of O and C in high order number 'n' are interspersed through the Ti and Fe ion emission.

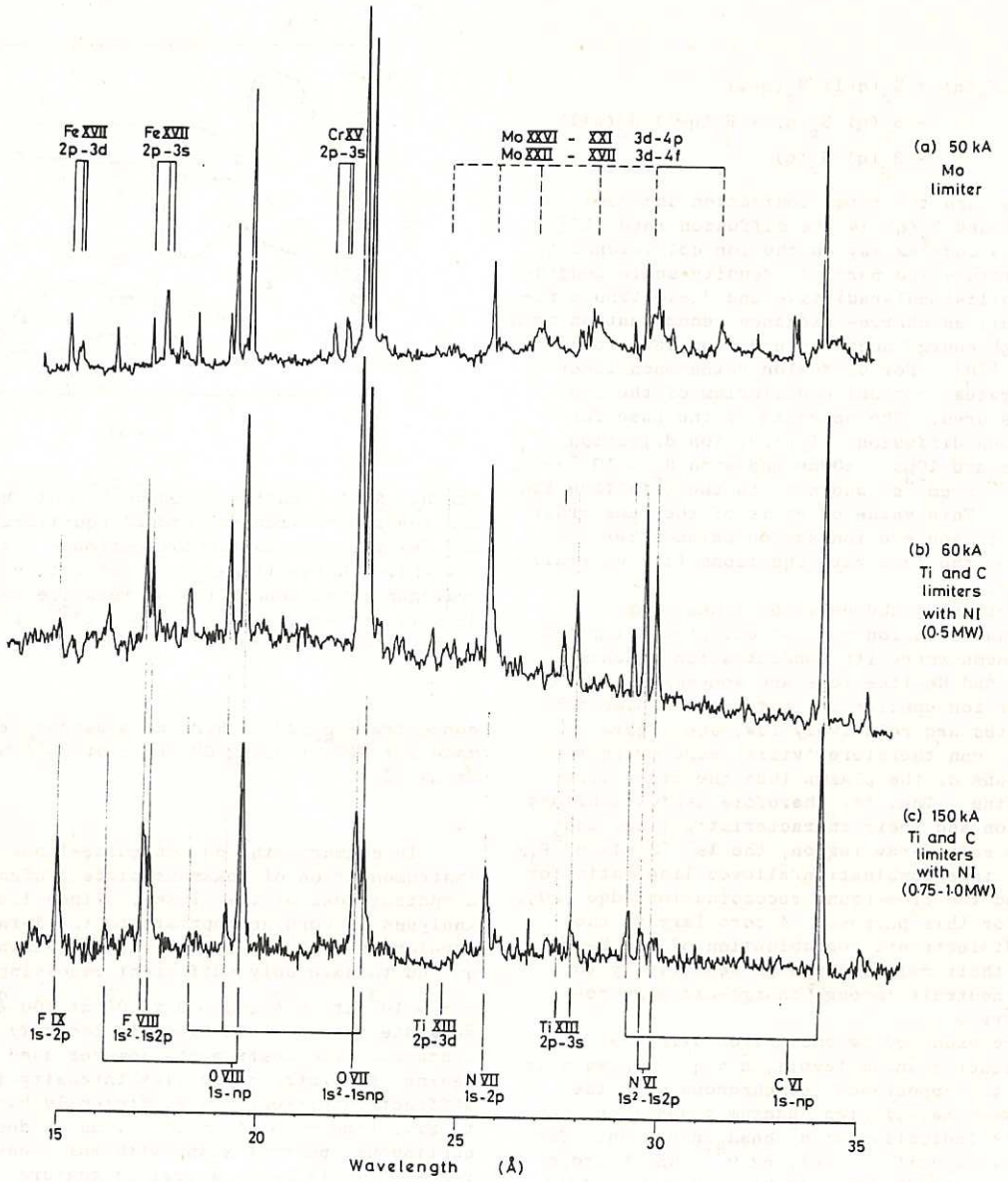

Fig 4. Section of soft X-ray spectrum (15 Å - 35 Å) from DITE tokamak. Three different operating conditions are shown. In (a) the discharge is ohmically heated (50 kA current) and the current aperture limiters are Mo. In (b) and (c) the limiters are Ti and C while the plasma ohmic heating current and neutral injection (NI) power are as indicated.

ween levels within the ground configurations lie ically in the VUV region of the spectrum.

Δn > 0 transitions of the common metals whose ions isoelectronic with carbon or with any other ion in neon-shell, (ie the so-called M-shell transitions), in the soft X-ray region. In this region of the ctrum, ∿ 10 Å → ∿ 100 Å, the Δn > 0, M-shell metal es form a well separated group from the Δn = 0 lines indicated in figure 1, and interspersed through these groups are the K-shell Δn > 0 resonance lines of ised light impurities. Figure 3 illustrates a section the spectrum near 100 Å from the DITE tokamak: the n line features are from ionised Ti and Fe. The most ily charged states of the metals observed in these charges with Te(o) ≈ 800 eV were TiXX and FeXXI. sion at the shorter wavelengths, around 25 Å in the X-ray region, is illustrated for a number of dif- nt DITE plasma conditions in figure 4. It is worth ng that with more limited resolution the FeXVII d, 3s multiplets (upper trace) between 15 Å and 17 Å d easily be confused with the FIX and FVIII lines which appear at or near the same wavelengths during neutral beam injection (lower trace). A resolution interval of 0.1 Å or better is desirable therefore in this wavelength region.

Very high resolving power, sufficient to undertake line profile studies, is difficult to achieve with grating dispersion at grazing incidence. Instrumentation for line profile analyses is more easily achieved using crystal dispersion at shorter wavelengths or with normal-incidence gratings at much longer wavelengths. Of more interest in tokamak physics is the absolute soft X-ray photon fluxes from which are derived the spatial concentration of the impurity ions since these influence the overall energy balance and even plasma stability [16]. Impurity ion transport in tokamaks is a complex problem and depends on particle diffusion coupled with the atomic rate coefficients, viz,

$$\frac{\partial N_z(q)}{\partial t} + \nabla D_z(q) \nabla N_z(q) = S_z(q-1)\, N_z(q-1) - S_z(q)\, N_z(q) + R_z(q+1)\, N_z(q+1) - R_z(q)\, N_z(q) \quad \ldots (1)$$

where $S_z(q)$, $R_z(q)$ are the total ionisation and recombination rates and $D_z(q)$ is the diffusion rate [17] which depends in a complex way on the ion collisionality, and on the temperature and particle density scale lengths. $R_z(q)$ includes collisional-radiative and dielectronic recombination as well as charge- exchange recombination from both injected high energy neutrals and from background thermal neutrals [18]. For diffusion rates much lower than the atomic rates, coronal equilibrium of the ion populations is assured. The opposite is the case for relatively fast ion diffusion. Typical ion diffusion times in tokamaks are 10ms → 100ms and with $N_e \sim 10^{13}$ cm^{-3}. $n_e \tau_c \simeq 10^{11} \rightarrow 10^{12}$ > cm^{-3} s, where τ_c is the effective ion confinement time. This value of $n\tau_c$ is of the same order as that required to achieve ionisation balance between the ion species so the full rate equations (1), generally need to be solved.

Space resolution of the emission lines from tokamaks shows that each ion species occupies a limited volume of the plasma where its concentration reaches a maximum. H-like and He-like ions are somewhat anomalous relative to other ion species in that their dielectronic recombination rates are relatively low, see figure 5. These ion species can therefore 'visit' more extensive temperature regions of the plasma than the other ions, without recombining. They are therefore useful monitors of ionic diffusion and their characteristic lines and continuua in the soft X-ray region, the $1s^2\ ^1S_o$-$1s2p\ ^3P_1$/ $1s^2\ ^1S_o$-$1s2p\ ^1P_1$ intercombination/allowed line ratio for example [19], and the free-bound recombination edge [20], have been used for this purpose. A corollary to the relatively low dielectronic recombination of the H-and He-like ions is their relatively high sensitivity to the presence of neutrals through charge-exchange recombination, figure 5.

Since charge exchange recombination directly populates the higher quantum levels, $\bar{n} \simeq q^{0.77}$ where q is the ion charge, the appearance, synchronous with the beam current rise-time, of high quantum transitions in impurity ions, is indicative of H^o beam injection. The concentrations of impurity nuclei, eg O^{8+}, which ordinarily are difficult to detect, can be measured in this way[21]. The emission rate, neglecting cascades from the upper levels, is simply,

$$I_{jk} = N(H^o)\, V_b \sigma_{chx}\, N(O^{8+}) \frac{A_{jk}}{\sum_{k=j-1}^{1} A_{jk}} \quad \ldots (2)$$

where V_b is the beam velocity.

While, per charge exchange collision time (which equals the ionisation time in a steady-state beam-injected plasma), the population of the n = 2 level of OVIII might increase by a factor of about two or less due to charge transfer from O^{8+}, (electron impact excitation always being a heavily competing process for low quantum states) the population of the upper levels, in contrast, can have their relative population increased by well over an order of magnitude due to charge exchange. Typically, OVIII H_α will be enhanced during the beam injection pulse by a factor of 20 or more relative to its intensity prior to beam-injection. The Ly-α line of OVIII at 19Å remains, therefore a good monitor of changes in the ground state population and thus of the ionisation balance, while the H_α doublet at 102.37, .51 Å is more useful for monitoring and mapping out the H^o particle beam penetration into the plasma. Isler [22] was the first to recognise the implications of the steep increase in OVIII H_α during H^o beam injection into tokamaks. More recently he has used the prompt radiation from the O^{8+} 5-4 transition in OVIII at 632 Å to measure the O^{8+} concentration [23]. Similar measurements have been made for $N(C^{6+})$ using CVI Ly-α at 33 Å by Afrosimov et al [24].

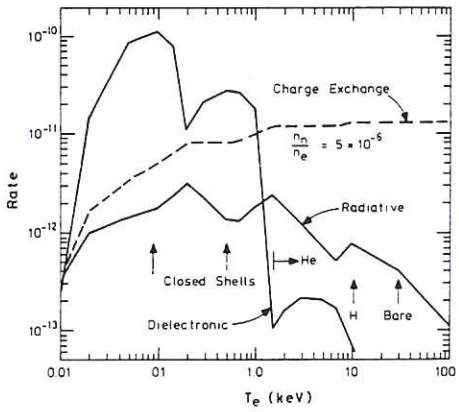

Fig 5. Recombination rates(em^{3}s^{-1}) of the most abundan ion species of Iron in coronal equilibrium. For the H- and He-like species the dielectronic rates are relativ low while charge transfer recombination from neutral hydrogen whose concentration relative to the electron density is taken as $n_n/n_e = 5 \times 10^{-6}$, is relatively large. (D E Post and R A Hulse, PPL).

In summary, the design guide-lines for soft X-ray instrumentation of tokamaks place a high priority on a spatial scan of the plasma. Since line profile analyses is more appropriate to the X-ray and VUV wavelength regions, soft X-ray instruments are required to have only sufficient resolving power. $\frac{\lambda}{\Delta\lambda} \sim 10^3$ at 10 Å and $\sim 3 \times 10^3$ at 100 Å, in order to separate out and unambiguously identify the line features. The instruments however need to be calibrat against absolute photon flux intensity falling on the diffraction element. A sufficiently high aperture to give time resolution of ∿ 1 ms is desirable, while continuous spectral scans with multi-channel electroni read-out would be an appealing feature.

Because of the large plasma dimensions, typically 0.1m to 1m, X-ray imaging systems such as coded apertures or grazing incidence focusing optics are less useful than tomographic analyses of the line-of-sight, chordal, soft X-ray fluxes. The derivation of spatial plasma profiles at PPL, Princeton University [25], using surface barrier detector arrays which simultaneously and continuously view as many as 20 chords through a tokamak has very adequately demonstrated the power of this technique. Nevertheless, a simple pinhole imaging system with image intensifier cameras and I-D electronic read-out with framing rates of 50 KHz h been proposed for tokamak diagnostics [26].

B. Laser-Produced Plasmas

Irradiation of solid targets by intense laser bea has produced approximately the same range of ion speci as has magnetically confined plasmas. By 'tailoring' light irradiation intensity at the target surface it i possible to replicate the ionic emission from tokamaks figure 6.

Using 1μm laser light with a critical density for total light reflection of 10^{21} cm^{-3}, a flux intensity o $\sim 10^{15}$ wcm^{-2} at the target surface will produce an elec tron temperature, kTe ∿ 1 keV, and light atoms, eg O, N etc in the critical density layer, will be stripped typically of all their electrons. The common metals appear as He- and Li-like ions while heavier elements, such as Au, can lose some 50 or more of their outer electrons.

In contrast to magnetically confined plasmas however, the interesting physics of the laser interaction, such as the light absorption, energy balance, and heat and particle transport into the solid, takes place in a highly constricted space and time scale. Measurements with 10 ps (temporal) and 1μm (spatial) resolutions are desirable. Collision processes are extremely rapid $\sim 10^{11}\,s^{-1}$ so that radiative decays from metastable levels are not observed. For example, the $3d^n$-$3d^{n-1}4s$(E2) forbidden lines of MoXVI and MoXV, which have A values of $\sim 10^7\,s^{-1}$ and are strong features of the Mo spectrum in a tokamak, are absent in laser irradiated Mo-targets, figure 6.

Despite the high collision frequency, ionisation-recombination equilibrium is not a general rule in laser-matter interaction experiments. This is due to the steep density gradients ($\ell_s \gtrsim 1\mu m$) where ℓ_s is the density scale length, the (less severe) temperature gradients, and the high streaming velocity, $V_{iz} > 10^7\,cm\,s^{-1}$, of the plasma as it expands away from the laser energy deposition layer. The effective ion confinement time $\tau_{iz} \sim (n_e R_z(q))^{-1}$ and the value of the confinement parameter $n_e \tau_{iz} (n_e \ell_s / V_{iz}) \simeq 10^{10}\,cm^{-3}\,s$ are less than those necessary to achieve ionisation balance [27].

The main diagnostic parameters of interest in laser-plasma interactions or laser-driven compression experiments are the spatial density structure in the inter-action region and the compressed core density and the confinement factor $\int \rho.dr$. These parameters and $\int \rho.dr$ can be derived conveniently from line broadening. Linear Stark broadening of H-like transitions in these high density plasmas is often of the order $\Delta\lambda_s/\lambda \sim 10^{-2}$ so that ions, eg Ar XVIII, seeded into the compressed plasma, emit lines which can act as density indicators. The use of linear Start broadening is restricted not only to hydrogenic (degenerate) levels but in practice is often restricted, also, to intermediate quantum levels. High quantum transitions merge with the continuum while transitions from the lowest quantum levels are often optically thick to line radiation. An optical depth τ_o for Ly-α can often be between 10 → 100 while for Ly-β a value of $\tau_o \sim 1$ is more usual. It is important to note that a single observable such as the half intensity width of an optically thick line is not of itself a unique function of the plasma microfield broadening and therefore of n_e but depends also on the number density of the emitter ions [28]. More appropriately, the series members such as Ly-α, -β are used to derive the product of the emitter concentration and scale length, ie $\int \rho.dr$, from their opacity-distorted profiles, while the optically thin, higher series members eg Ly-γ and Ly-δ and H_α which all suffer mainly Stark broadening, are used to derive ρ.

Crystal instruments are most often used for line profile analyses at $\lambda < 25$Å [28] [29], although the plasma microfield broadening of the optically thin line wings can be sufficient at longer wavelengths to contemplate the use also of grazing-incidence grating dispersion [30]. Space resolution is simply but inefficiently effected by positioning an aperture between the plasma and dispersion element or between the input slit and the dispersion element in the case respectively of a crystal or a grating spectrometer. Relay focusing optics using grazing-incidence mirrors allows the spectrometers to be remotely positioned from the plasma. When considering X-ray imaging systems [8] [31], coded-aperture and reflection-optics microscopy allow a large increase in the soft X-ray throughput (for a given spatial resolution) over that available with a pin-hole aperture. Time-resolution of the soft X-rays is now routinely achieved by projecting an X-ray image or spectrum onto the photocathode of a gated, image-intensifier. These cameras have inherent resolutions of 1ps and 20 ℓ/mm. Remarkable advances have been made, during recent years in the diagnostics of these highly transient micron-size plasmas [31]. However, a combination of high light throughput, time resolution ∼ 10ps space resolution ∼ 1μm and spectral resolution $\frac{\lambda}{\Delta\lambda} >> 10^3$, is still something of a tour de force.

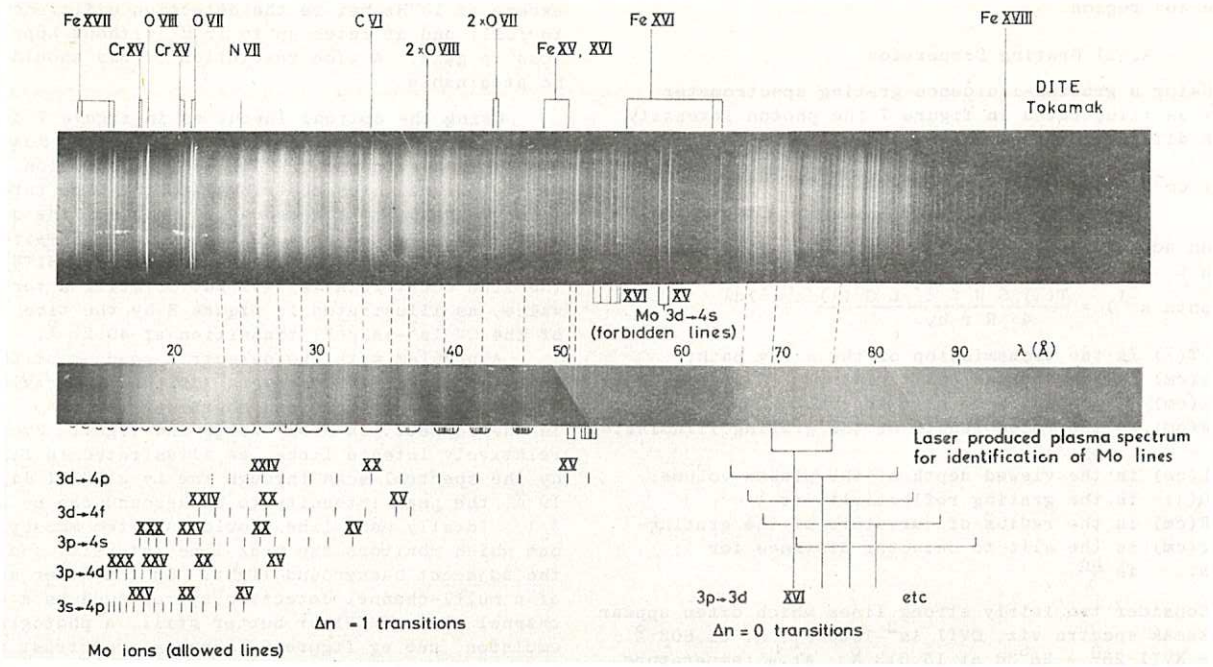

Fig 6. Soft X-ray spectrum from DITE tokamak operated with a Mo limiter (upper) compared with spectrum from laser-irradiated solid Mo target(lower). Note the appearance of the Mo forbidden lines in the tokamak spectrum.

III DESIGN CRITERIA FOR SOFT X-RAY INSTRUMENTATION

A. Tokamaks

In the design of dispersion instruments for fusion studies it is pertinent to consider firstly the intensity of the emission lines from the plasma and secondly the throughput efficiency required of the spectrometer to achieve a desired time or spectral resolution. The volume emissivity of a line is simply

$$\int \varepsilon\ (\lambda)\ d\lambda = \frac{N_z(q_j)\ A_{ij}\ h\nu_{ij}}{4\pi} \qquad \ldots\ (3)$$

The local concentrations of the ions of atomic number Z and charge state q is often the parameter of interest. The population of level j can be calculated in terms of the ground state population using appropriate numerical codes [32] which include the collisional and radiative coupling processes between a significant fraction of all the levels, including levels i and j. More simply, the coronal relation can sometimes be used.

$$\int \varepsilon\ (\lambda)\ d\lambda = \frac{n_e N_z(q_{ij})\ C_{ij}\ \frac{A_{ij}}{\sum_j A_{ij}}\ h\nu_{ij}}{} \qquad \ldots\ (4)$$

where the excitation rate is given in terms of the collision strength Ω_{ij},

$$C_{ij}\ (cm^{-3}s^{-1}) = \frac{8.63 \times 10^{-6}}{\omega_i (kTe)^{3/2}} \int_{\Delta E_{ij}}^{\infty} \Omega_{ij}(E)\ \exp(-E/kT_e)\,dE \qquad \ldots\ (5)$$

This relation is appropriate to allowed transitions whose upper levels are populated entirely by collisions from the ground level and where branching decays are known. The presence of metastable levels coupled to the upper level can disqualify this simple coronal excitation model, in which case one has to fall back on a numerical solution of the full set of time dependent coupled equations describing the level populations.

Volume emissivities of strong impurity lines from tokamaks range typically from $\sim 10^{10}$ photons $cm^{-3}s^{-1}$ in the X-ray region to $\sim 10^{15}$ photons $cm^{-3}s^{-1}$ in the XUV region.

A.(i) Grating Dispersion

Using a grazing-incidence grating spectrometer layout as illustrated in figure 7 the photon intensity in the diffracted lines can be calculated

$$F(\text{ergs cm}^{-2}\text{s}^{-1}) = \frac{T\ (\lambda)\ S\ W\ \ell\ L\ G(\lambda)}{4\ R.\ r.\ dx_{1/2} \sin\beta} \int \varepsilon(\lambda) d\lambda \qquad \ldots\ (6)$$

With an acceptance slit width $s' = dx_{1/2} \sin\beta$ and length ℓ' at the detector, then

$$F'(\text{quanta s}^{-1}) = \frac{T(\lambda)\ S\ W\ \ell\ \ell'\ L\ G\ (\lambda) \int \varepsilon\ (\lambda) d\lambda}{4\pi\ R\ r\ h\nu} \qquad \ldots\ (7)$$

where $T(\lambda)$ is the transmission of the λ ray path;
s(cm) is the entrance slit width;
ℓ(cm) is the entrance slit length;
W(cm) is the ruled length of the grating illuminated by λ;
L(cm) is the viewed depth of the plasma volume;
$G(\lambda)$ is the grating reflectivity at λ
R(cm) is the radius of curvature of the grating-
r(cm) is the slit to detector distance for λ;
$h\nu$ is $\frac{hc}{\lambda}$

Consider two fairly strong lines which often appear in tokamak spectra viz, OVII $1s^2$-$1s2p^1P_1$, at 21.602 Å and Fe XVII $2p^6$ - $2p^5$3d at 15.013 Å. At a temperature of 300 eV the fractional abundance of O^{6+} is ~ 0.1. Thus for $n_e = 3 \times 10^{13} cm^{-3}$ and a typical oxygen impurity level of 1%, $\Sigma_q N(O^{+q})/n_e = 0.01$, then $N(O^{6+}) = 3 \times 10^9 cm^{-3}$ and $\int \varepsilon(21.6\ Å)\ d\lambda = 1.6 \times 10^{13}$ ph $cm^{-3}s^{-1}$. At a temperature of $\sim$ 400 eV when Fe XVII has a relatively high fractional abundance, $N(Fe^{+16})/\Sigma_q^{26} N(Fe^{+q}) \simeq 0.5 \rightarrow 0.6$, and at the same electron density, $3 \times 10^{13} cm^{-3}$, and an iron impurity level of 0.001 n_e, then

$$\int \varepsilon\ (15\ Å)\ d\lambda = 3 \times 10^{13} \text{ ph cm}^{-3}\ \text{s}^{-1}$$

Setting, appropriate values for the symbols in equation (7) we derive for the flux in the diffracted line

$$F'(21.6\ Å) = \frac{1.0 \times 0.001 \times 2.0 \times 0.75 \times 1.0 \times 50 \times 0.05}{4\pi \times 200 \times 25} \quad \frac{1.47 \times 10^{4}}{0.919 \times 1}$$

$$\simeq 1 \times 10^6 \text{ quanta s}^{-1}$$

Taking a quantum efficiency of 5%, typical of a channeltron response at $\sim$ 21 Å, the above flux gives a count rate of 5×10^4Hz. The count rate for the Fe XVII (15 Å) line is nearly the same. Assuming an electron multiplication of 10^7, the charge collection rate is $\sim$ 0.08μA for these soft X-ray lines. High count rate channeltrons such as the "Galileo 4818" can operate in excess of 10^6Hz before the detection efficiency starts to fall, and at rates up to 10^5Hz without appreciable loss in gain. A time resolution of 5ms should therefore be attainable.

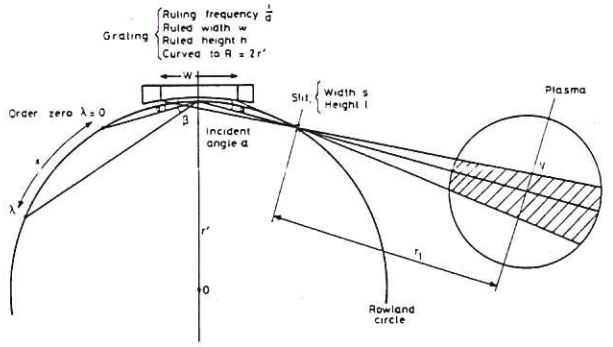

Fig 7. Schematic diagram of the optical layout of a Rowland circle grazing-incidence grating spectrograph viewing the cross section of a toroidal plasma.

Using the optical layout as in figure 7 one might then expect count rates of up to 10^5Hz for most of the intense lines in the grazing incidence region. The depth of the plasma which contribute to the line intensity is taken to be 0.5m, a reasonable value for the dimensions of the sub-keV temperature region in a JET-sized tokamak. In a smaller device such as the DITE tokamak the line count rate is less but is still a very useful value, as illustrated in figure 8 by the time variation of the CV $1s^2$-$1s2p^1P_1$ transition at 40.27 Å.

A problem with photoelectric readout of the spectra which is particularly severe for shallow grazing angles of the incident light and short wavelengths, $\lambda < 100$ Å, is the competition from background light. Even for relatively intense lines, as illustrated in figure 9 by the spectral scan through the Ly-α OVIII line at 19 Å, the peak intensity to background can be as low as 3/1. Ideally each line should have two measuring channels one which monitors the peak line intensity and the other the adjacent background light. On the other hand, use of a multi-channel detection system such as a micro-channel plate (MCP) or better still, a photographic emulsion, see eg figure 6, ensures a contrast of at least 20/1. The source of this background light has not been properly researched but is probably due to scattered soft X-rays or longer wavelengths scattered from the grating, perhaps also fluorescence of the grating to harder X-rays. Channeltrons are a poor choice of detec

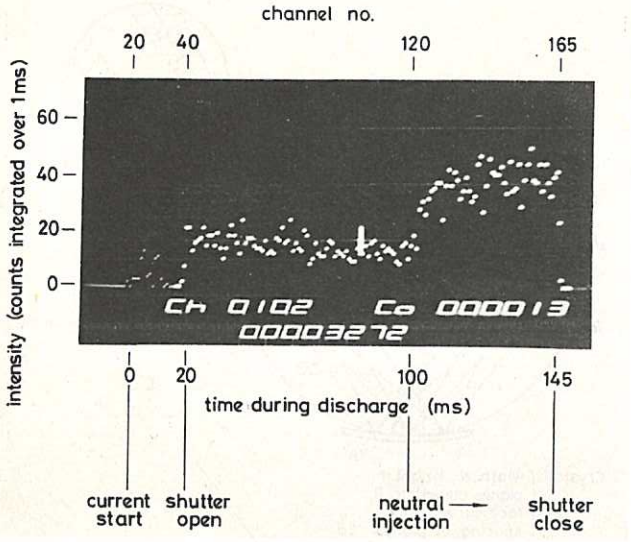

Fig 8. Time variation of CV $1s^2$-$1s2p.\ ^1P_1$, 40.27 Å emission from the DITE tokamak, measured with a grazing-incidence spectrometer. Note the increased level during the neutral injection pulse and negligible background detector signal with the mechanical shutter closed.

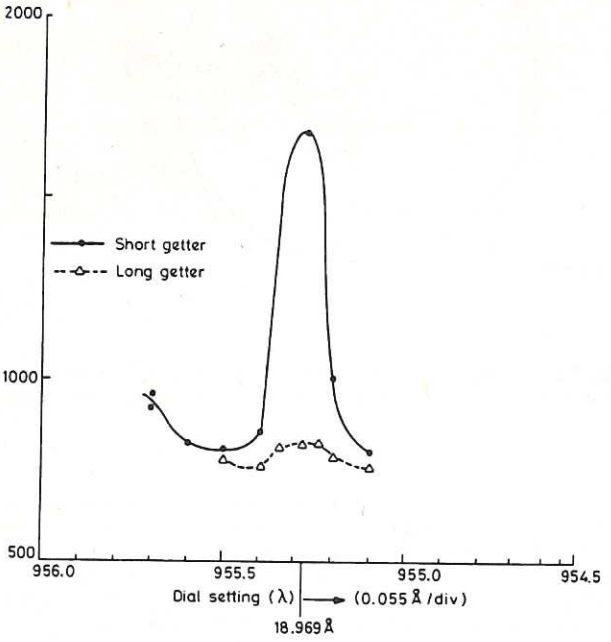

ig 9. Wavelength scans, on successive discharges of he DITE tokamak, through the Ly-α OVIII emission. The long getter' pulsed conditions reduce the oxygen oncentration and the emission from this ion falls to lmost the background light level.

in the respect that they are sensitive to a wide range of wavelengths with a peak sensitivity in the XUV spectral region. The use of filters [33] and low scatter, holographically ruled gratings help to increase the line intensity/background ratio but it is very difficult to realise the same contrast over a broad spectral band as is routinely achieved with photographic emulsion. Our calculations indicate, moreover, that to achieve a density of 0.5 above fog on, say, Kodak Pathe SC-5 film with the photon flux estimated (above) for OVII at 21.6 Å (using a 2 metre radius grating ruled with 1200 1/mm at a 2° grazing angle) an exposure time of ∿ 250ms is required. For very long-lasting plasmas such as anticipated in the JET tokamak (∿ 10s) the use of a grazing-incidence spectrometer with photographic emulsion recording and with a camera shutter to control the exposure time is not an unappealing proposition.

A(ii) Crystal Dispersion

At wavelengths shorter than about 25 Å, crystal dispersion becomes an alternative to the use of grazing incidence diffraction gratings. Crystals are highly effective monochromators rather than true broad band spectrometers, so that surveying a region of the spectrum conventionally involves scanning the crystal through a range of Bragg angles, either stepping the angle in a series of discrete motions or by continuous crystal rotation. If a flat crystal is used, reasonable spectral resolution can be maintained by restricting the angular divergence of the incident light at the crystal with a Soller slit. Indeed, the first crystal survey of a plasma in the soft X-ray region (λ < 22 Å) was achieved with just such a flat crystal and Soller slit arrangement [34]. An alternative arrangement is to accept a range of Bragg angles simultaneously by the crystal convex in the "de Broglie" configuration, figure 12.

A large increase in light throughput with higher resolution can be achieved if the crystal is bent, in the "Johann" mode, concave to the diameter of a Rowland circle onto which is positioned the effective entrance aperture, the dispersion element and the detector. Better efficiency still can be achieved if the Rowland circle arrangement is retained but with the front face of the crystal ground to the Rowland circle radius as in the fully-focusing "Johansson" mode. The relative merits of these convex and concave configurations for tokamak (JET) studies are discussed by Hobby et al [35].

The schematic optical layout of a focusing crystal spectrometer attached to a toroidal plasma device is shown in figure 10 with the Rowland circle parallel to the toroidal axis. The wavelength coverage ie the range of Bragg angles is clearly dependent on the entrance aperture to the torus and on the diameter of the Rowland circle. Our proposal [35] for the JET tokamak studies favours a relatively small Rowland circle diameter R = 75 cm and a compact vacuum system. The crystal width W can then be kept reasonably small < 5cm, while the sensitivity is not affected since this depends on W/R. Defocusing aberrations on the other hand scale as $(W/R)^2$ and $(h/R)^2$ where h is the crystal dimension orthogonal to the plane of the dispersion but these will lead to only a marginal loss in resolution [35].

One consequence of the relatively tight focusing circle is the requirement for a high spatial resolution detection system. Microchannel plates provide adequate resolution (∿ 0.035mm) for this purpose and we tolerate their rather poor efficiency ∿ 5% → 20% over the range 10 Å → 100 Å in the soft X-ray region. In order to cover the important line groups from the ion species likely to be present in a tokamak, a stack of six different crystals is proposed [35] viewing the plasma over a range of Bragg angles from 48° to 58 Å. A high mean viewing angle ∿ 53° is preferred for low optical aberration, high resolution and near normal-incidence on the detectors. The microchannel plates have a 30° bias of the channels to the normal as indicated in figure 11 in order that the diffracted light strikes the channels at an optimum angle ∿ 7°

for maximum sensitivity.

The resolving power of the crystal instrument is

$$\frac{\lambda}{\delta\lambda} = \frac{\tan\theta_B}{\delta\theta} \qquad \ldots (8)$$

where $\delta\theta$ is a convolution of $\delta\theta_R + \delta\theta_h + \delta\theta_D$. $\delta\theta_R$ is the FWHM of the crystal diffraction pattern, $\delta\theta_h$ is the focusing aberration, $\delta\theta_D$ is the loss in resolution due to the finite elements of the detector.

For the spectrometer characteristics outlined above we might expect a resolving power of between 10^4 and 2×10^4 for dispersion of 2 Å light from a good quality quartz crystal [35]. Since in the soft X-ray region we are interested in rather longer wavelengths, then mica could be used to diffract 15 Å radiation at a Bragg angle of 48.9° (ie within the angular viewing range of the instrument). The crystal diffraction width for 15 Å light in first order from a mica crystal is likely to be ∿ 100 arc sec and this is at least an order of magnitude wider than diffraction widths for good quality crystals in the X-ray region proper. The resolution therefore at these longer wavelengths is proportionately reduced.

As for the Rowland circle grating instrument, we can calculate the sensitivity relation for the Johansson configuration, viz.

$$P = T(\lambda)\,\frac{W\,h\,L\,R(\theta_c)}{4\,\pi\,R\,dx_{1/2}}\,\frac{\int\varepsilon(\lambda)\,d\lambda}{h\nu} \qquad \ldots (9)$$

where the symbols are as equation (6), except that $R(\theta_c)$ is now the integrated reflectivity of the crystal.

For a detector length ℓ' and width $(dx)_{1/2}$ the flux in the diffracted line is

$$P' = T(\lambda)\,\frac{W\,h\,L\,R(\theta_c)\,\ell'\int\varepsilon(\lambda)d\lambda}{4\,\pi\,R\,h\nu}\ \text{(quanta s}^{-1}\text{)} \qquad \ldots(10)$$

Again, considering as before the Fe XVII line at 15.013 Å from a plasma with the same parameters and the same volume emissivity $\int\varepsilon(\lambda)\,dx = 3 \times 10^{13}$ ph cm^{-3}s^{-1}; but now assuming mica crystal dispersion with $R(\theta c) = 10^{-5}$, and a detector length of 1cm, we have,

$$P'\ (15\ \text{Å}) = \frac{1.0 \times 4.0 \times 1.0 \times 50 \times 1 \times 10^{-5} \times 1.0 \times 3 \times 10^{13}}{4\,\pi \times 75}$$

$$= 6.4 \times 10^{7}\ \text{quanta s}^{-1}$$

For a detector efficiency of 4% this represents for the 15 Å line a count rate of 2.6×10^6 Hz (∿ 1×10^8 electrons cm^{-2}s^{-1} at the detector surface). Such an instrument should provide time-resolved impurity spectra from a Jet-size plasma on the time scale of a few msecs.
A cascaded channel-plate assembly with delay-line read-out satisfies most of the detector requirements giving adequate spatial resolution and quantum efficiency, though probably the dynamic range is insufficient to record the strong lines synchronously with the very weak lines.

The use of much larger radius focusing crystal instruments, for example the 3.3m Johan configuration with multi-wire proportional counter read-out used at Princeton University, has already proved very effective for line profile studies of tokamak plasmas [36]. Other intermediate-size configurations, such as the 1.5m Johann spectrometer at Fontenay aux Roses [37], with the quartz crystal held against the cylindrical former by atmospheric pressure and with linear, position-sensitive proportional counter read-out, have also been developed. The tighter Rowland circle proposed here [35] suffers in no important respect such as light throughput, resolution etc, while its compact size allows it to be tilted so as to spatially scan the plasma volume.

For soft X-ray spectral survey purposes a very

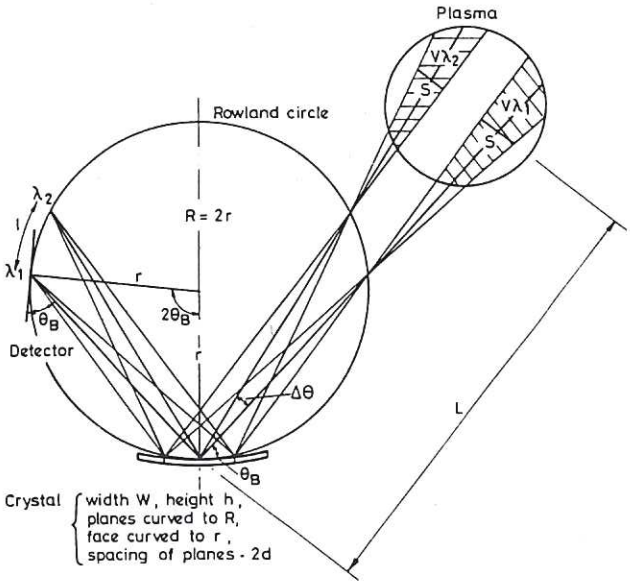

Fig 10. Schematic diagram of the optical principle of the Johansson focusing crystal spectrometer.

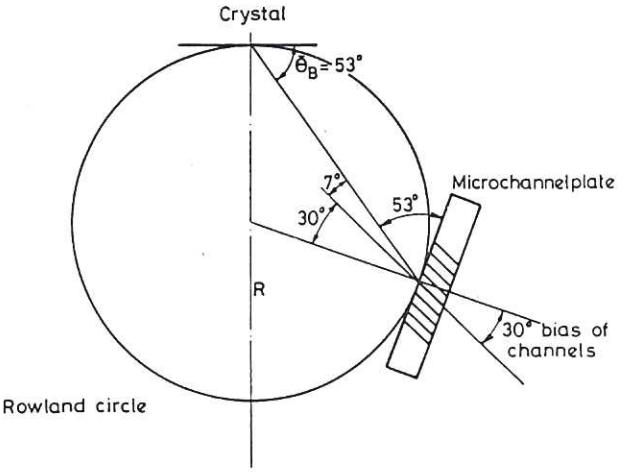

Fig 11. Tangential setting of special 30° bias micro-channel plate for optimum efficiency (glancing angle 7°

simple crystal spectrometer can be based on the de Broglie convexly curved configuration, figure 12. This spectrometer can be used with photographic or photoelectric read-out, and with a curved KAP crystal wavelength coverage from 1 → ∿ 23 Å can be expected. The relative low efficiency of this configuration means that only modest time-resolution is achieved. The dispersion relation for the de Broglie configuration is

$$\frac{d\lambda}{d\ell} = \frac{2d\cos\theta}{R\left[2 - \frac{r\sin\theta}{R}\left(1 - \left(\frac{r\cos\theta}{R}\right)^2\right)^{-\frac{1}{2}}\right]} \qquad \ldots$$

where r is the crystal curvature and R is the radius of the detector circle around which the wavelength variation is almost linear with distance.

The count rate per emission line dispersed by the
e Broglie crystal viewing an extended source through a
arrow slit is given by

$$F' = \frac{T(\lambda)\, r \sin\theta\, R(\theta_c)\, s\, b\, L\, \ell' \int \varepsilon(\lambda)\, d\lambda}{4\pi\, \ell\, (\ell + t)\, h\nu} \quad \text{(quanta s}^{-1}\text{)} \qquad \ldots\ldots(12)$$

here the symbols have the same meaning as before except,
θ is the Bragg angle for wavelength λ;
(cm) is the curvature of the crystal;
(cm) is the distance of the slit to the crystal;
(cm) is the distance from the slit to the detector;
(cm) is the slit width and b (cm) is the slit length;
Again, assuming a de Broglie spectrometer with a
ica crystal, 5 cm high, viewing a 50 cm depth of a
okamak plasma which emits 3 x 10^{13} photon cm^{-3} of 15 Å
e XVII light then inserting appropriate numerical
alues for the symbols respectively in equation (11),

$$F' = \frac{..0 \times 5.0 \sin 49^\circ \times 10^{-5} \times 0.05 \times 5 \times 50 \times 1.0 \times 3 \times 10^{13}}{4\pi \times 50 \times 60}$$

$$= 3.8 \times 10^5 \text{ quanta/s}$$

hich, with a 4% photo-detection efficiency, gives a
ount rate of 1.5 x 10^4 Hz. With a global count rate [35]
or the channeltron read out system of ∿10^6Hz, several
ens of lines can be recorded with about 1% statistical
ariation and a fraction of a second exposure. Even with
hotographic film a density of 0.5 above fog would be
cieved with an exposure line ≳ 10 sec (ie the full
ulse length of the JET tokamak).
n alternative broad-band crystal configuration
akes use of a plane flat crystal which is rotated
hrough the required range of Bragg angles. Collimation
f the input light with grided apertures is necessary.
n this case the detector can be a simple light 'bucket'
nd the spectrum is dispersed as a function of time. A
x 5 cm crystal with a rotational speed of 100 Hz and
n acceptance angle of 100 arc sec set by the crystal
ocking curve and the entrance collimator would give a
otal count rate per line of the same order as the
tatic, de Broglie instrument. Comparing the merits of
hese two modes, the rotating and static crystals, there
s a direct trade off between band-width and time reso-
ution, the spectral resolution remaining almost constant
ore sensibly therefore the light throughput should be
ncreased at the expense of band-width by slowing the
otation to ∿ 1 Hz. These flat crystal configurations
re used with considerable success in stellar X-ray
tudies eg [38].

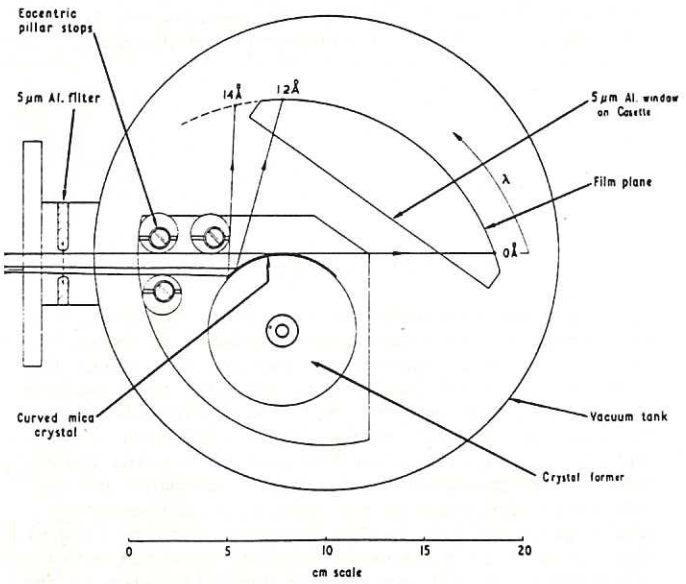

Fig 12. Optical layout of de Broglie crystal spectrometer.

A(iii) Crystal Versus Grating Dispersion
At Soft X-Ray Wavelengths

For wavelengths in excess of 25 Å, grating dispersion instruments have exclusively been used for broad band spectroscopy of fusion plasmas. At the short wavelength end of the soft X-ray region crystal instruments on the other hand have clear advantages in terms of light throughput and wavelength resolution. It is of interest to consider these parameters in the limited waveiength region ∿ 10 Å → ∿ 25 Å where the advantage of one dispersion system over another is somewhat contentious. An appreciation of the problem can be gained by considering the resolving power and light throughput of the focusing crystal and grating instruments cited for 15 Å light in sections III.A.(i) and (ii).

We note in A.(i) that a 10 μm slit width and a grating aperture of 2cm has been assumed in order to achieve a line flux ∿ 1 x 10^6 quanta s^{-1} at 15 Å. The resolution of the spectrometer is in this case determined largely by the slit width but also by the grating aperture and ruling frequency. At 15 Å a 10 μm slit presents no diffraction problems. The resolving power due to the finite slit width is,

$$R_{s\ell} = \left(\frac{\lambda}{\Delta\lambda}\right)_{s\ell} = \frac{\lambda\ 0.09\ R(m)\ n\ d\ (mm)}{s(\mu m)} \qquad \ldots(13)$$

where the symbols are as before, but with units in parentheses, n is the order number and d^{-1} is the grating ruling frequency. With a 2-metre radius of curvature and $d^{-1} = (2{,}400/mm)^{-1}$ then the slit width limited resolving power is given by

$$R_{sl} = \left(\frac{\lambda}{\Delta\lambda}\right)_{sl} = 654$$

The resolving power set by the grating aperture at grazing incidence is given by $R(opt) = \frac{0.92}{d}\, n \times W(opt)$

where the optimum aperture [39] is ∿ 1.2 cm for the above grating used at a 2° grazing angle.

The finite thickness of the emulsion also causes some loss in resolution. The overall resolving power however is largely determined by equation (13) and can be taken as < 1000. On the other hand we have seen, equation (8), that the resolving power of a Johann crystal spectrometer is largely dependent on the angular divergence $\delta\theta_R$ at the crystal which will support monochromatic Bragg reflection. For diffraction of 15 Å light from a mica crystal at a mean Bragg angle of 49°, $\delta\theta_R$ ∿ 100 arc sec, giving a resolving power

$$R(\theta_R) = \left(\frac{\lambda}{\delta\lambda}\right) = 2.3 \times 10^3.$$

Defocusing aberrations are given by

$$\frac{\lambda}{\delta\lambda_W} = 8R^2 \tan^2\theta / W^2 \qquad \ldots\ldots(14)$$

and

$$\frac{\lambda}{\delta\lambda_h} = 8R^2 \frac{\sin^2\theta}{h} \qquad \ldots\ldots(15)$$

and account for resolutions, $\delta\lambda_W$ and $\delta\lambda_h$ due to the finite aperture length W and finite height h of the crystal. The overall resolving power ≃ $R(\theta_R)$ of the Johann instrument is about a factor of 3.5 better than the grating instrument at 15 Å and has, moreover, a light throughput (see III.A(i), (ii), which is greater by a factor of ∿ 60. These advantages of focusing crystals became more pronounced at shorter wavelengths provided that one chooses an appropriate crytal to preserve an almost constant Bragg angle. The indications are that the 'cross-over' wavelength at which focusing crystals and gratings have comparable performance is between 20 Å → 25 Å. In respect of total band-width, of course, a grating spectrometer used at shallow angle of incidence, ≲ 1°, will easily outperform a focusing crystal spectrometer.

B. Laser-produced plasmas.

Despite the minute plasma dimensions, $\lesssim$ 100 μm, and the short duration, $\lesssim$ 1 ns, of the 1 keV plasmas produced by intense laser irradiation of solid targets, the X-ray emission is sufficiently copious, typically a few percent or more of the incident laser beam power, that even the relatively inefficient grating and crystal dispersion instruments can be used [40]. A consequence of the need for micron-size space resolution, is that X-ray microscopy in one form or another is essential. A time resolution of $\sim$ 10ps implies that fast electronic gating, or high-frequency response detectors capable of handling 'pileup' pulses, is necessary.

B.(i) Grating Spectroscopy

Grating spectrometers with a slit aperture orthogonal to the entrance slit and placed between it and the grating can provide sufficient spatial and spectral resolution to diagnose the critical surface and ablated plasma regions of the irradiation target [30]. In order to collect adequate light flux however, the plasma source is placed typically a few mm from the entrance slit of the spectrometer. However, the use of aspheric reflection optics to relay the X-rays to the grating allows the spectrometer to be placed remote from the plasma. In the Rutherford laboratory laser programme, for example, toric surfaces with principle radii of 5m and 26mm are used both for the relay optics and for the grating substrate [41]. Spatial resolution of the object of 10μm and a spectral resolution of 30 mÅ at λ = 40 Å have been acheived with a toric substrate carrying holographically formed 'rulings' at a frequency of 1200 1/mm. The formation of a stigmatic image, of course, occurs only over a limited spectral bandwidth. Photographic recording is commonly used with these grating spectrometers because there is little loss in resolution due to the emulsion thickness. Also it is often possible to map out a crude time history of the plasma expansion using the close correlation between the location of emitting ions and time.

B.(ii) Crystal Spectroscopy.

Focusing crystals, as in the Johann configuration, give little advantage over a flat crystal when viewing laser-produced plasma since the tight radius of curvature, $\sim$ 1 cm, required for light collection would induce unacceptable diffracted image aberrations. Miniature flat crystal spectrometers are most frequently used the spectral resolution being set by the crystal rocking curve and/or the finite size of the source. Fortunately, some diagnostic observables, such as Stark line widths of hydrogenic transitions, can be so large that the ultimate in spectral resolution is not required. In these crystal spectrometers a slit aperture, placed between the source and the film, figure 13, allows the plasma to be space-resolved with a resolution, typically 3 → 20μm. The image of the outer shell wall in micro-balloon irradiation experiments is clearly separated from the X-rays emission from the compressed core plasma.

Temporal resolution of the X-rays is effected by projecting the spectrum onto the photocathode of gated image-intensifier as illustrated in figure 14. A time resolution $\sim$ 70 ps and a spectral resolution ($\lambda/\Delta\lambda$) $\sim$ 500 are typical of this type of apparatus [42]. For X-rays in the energy range $h\upsilon \sim 1 \rightarrow 10$ keV, the photocathodes are typically at 200 Å thick coating of Au on a Be substrate.A spongey coating of CsI of thickness 20 → 200 μm, depending on the X-ray energy, can increase the overall sensitivity of the camera by a factor of $\sim$ 20, the image being recorded either on film or digitally via a charge coupled device (CCD). Since one dimension of the image plane is reserved for the time sweep only a thin slice of the geometrical image of the plasma is displayed.

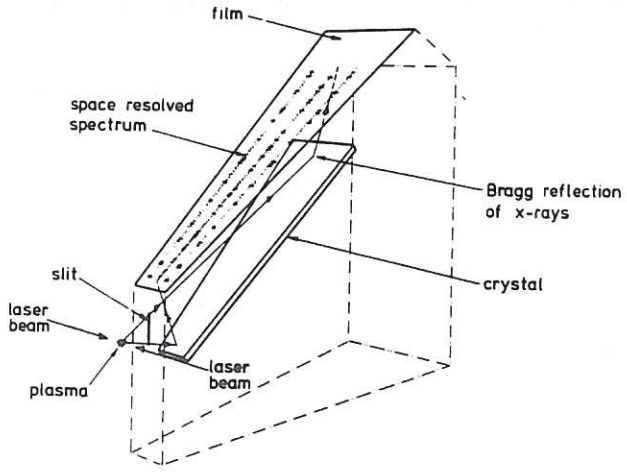

Fig 13. Flat crystal dispersion arrangement for spac resolution of the X-ray spectrum from laser-irradiate solid target.

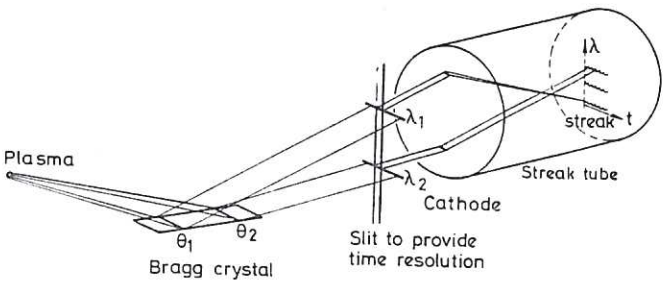

Fig 14. Schematic diagram of apparatus for X-ray streak spectroscopy of laser-produced plasma.

B.(iii) Soft X-ray Imaging Systems

In order to appreciate the extent to which X-ray microscopy of the minute plasma volumes produced in laser compression experiments has developed over the last few years one has only to refer to the Lawrence Livermore annual reports [43]. Reflection microscopy has the advantage of good spatial resolution $\sim$ 1 μm and relatively long objective distances which allows the image-forming components to remain undamaged during the micro-explosion of the target. A complementary technique developed by Ceglio and Co-workers [8][44][45] is that of coded-aperture imaging which gives the capability for 3-D analysis on reconstruction of the image. The coded apertures are typically free-standing micro Fresnel zone plates 5 μm → 25μm thick with zone

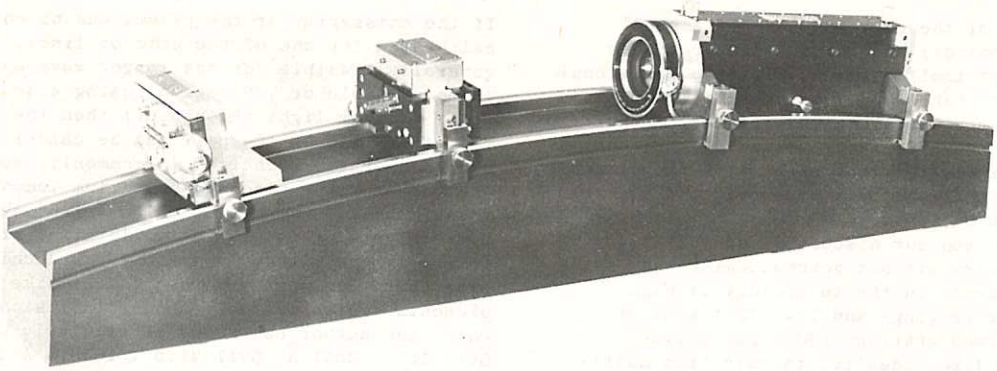

Fig 15. GML-5M grazing incidence spectrograph [51] showing entrance slit, grating and photographic cassette modules located on reference beam.

numbers 100 $\lesssim$ N $\lesssim$ 250, the width of the outermost zone being $\Delta r \simeq$ a few microns; this being the same order as the planar resolution. Tomographic (in depth) resolution of a few 10's of microns can be achieved. Thin transmission filters are employed, as in tokamak X-ray tomography [25], to differentiate between different regions of the spectrum - otherwise the apparatus developed for X-ray imaging of these two laboratory sources, tokamaks and laser-irradiated microballoons, could hardly be in more dramatic contrast.

IV. SOFT X-RAY SPECTROSCOPY AT THE CULHAM LABORATORY

Among the grazing incidence diffraction grating spectrometers at the Culham laboratory are a few which have seen continuous use since their design and construction some two decades ago. These include the E580, 3-metre instrument [46] which can be supplied,by Rank Hilger Ltd (UK), with photographic recording as in figure 4, or with a single-channel scan unit for photo-electric read out, figure 8. An earlier version of the present Mark III 3-metre spectrometer, with each of two scanning slits and associated photo-electric deflectors capable of being driven round the Rowland circle, was first used on the eta fusion device [47]. This illustrates the durability of the basic Rowland circle geometry for grazing-incidence grating spectroscopy.

A 'state of the art' development of these astigmatic instruments is the GLM-5 spectrograph (manufactured by Grating Instruments Ltd - UK) in which the slit, grating and detector modules are, within machining tolerance, located on the Rowland circle by virtue of their location on a one metre long segment of a reference circle [48]. This arrangement, gives flexibility in the disposition of the modules, as might be required, for example, in altering the angle of incidence, without degrading the preset focus. The basic instrument with photographic detector module is shown in figure 15 while a schematic diagram of the spectrograph in its vacuum tank, as it would be used to spatially scan a tokamak plasma, is shown in figure 16. Test spectra with a grazing angle of 1.65°, a holographically formed 600 1/mm grating, and a 1 μm entrance slit indicate a resolution of < 05 eV at $h\nu \simeq 150$ eV and < leV at $h\nu = 1.2$ keV. A channel scanning slit unit, figure 17, has been designed and fabricated [49] as an alternative photodetection module to the photographic cassette. The slit assemblies are symmetrical about a meridian dividing plane through the mid-point of the entrance slit and the pole of the grating, and they measure equal halves of the astigmaticaly lengthened spectral lines. Each slit is independently driven around the Rowland circle. This arrangement is ideal for line/background intensity measurements and for the measurement of line intensity ratios eg to Ly-$\alpha(O^{7+})/H_{\alpha}$ (O^{7+}) which are separated by $\sim$ 80 Å or for the intercombination/allowed lines of O^{7+} where the separation at 21.6 Å is only 0.2 Å.

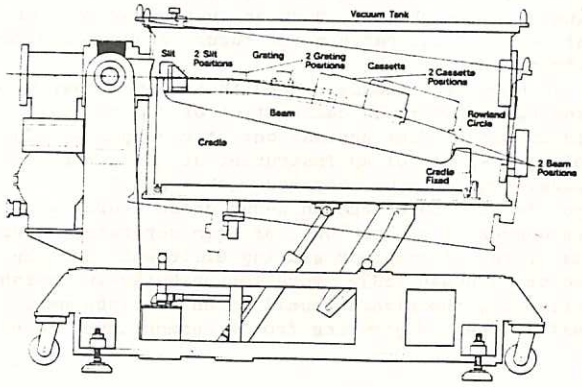

Fig 16. Optical layout of GML-5M grating spectrograph within vacuum housing. The whole assembly tilts to spatially scan the cross-section of a tokamak plasma.

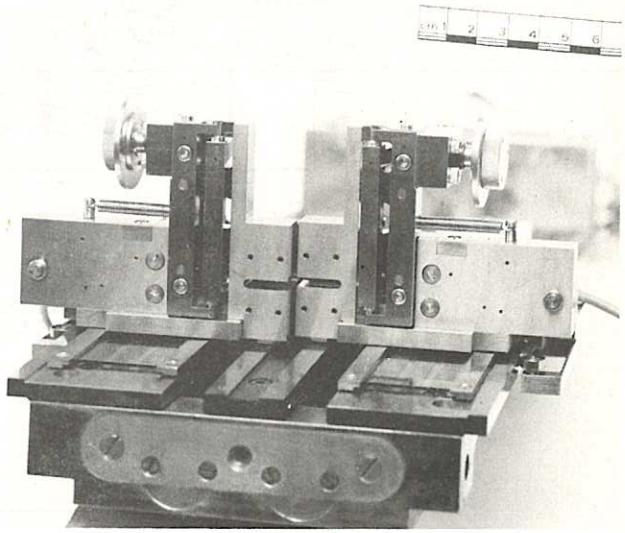

Fig 17. Two channel photo-electric detector module for GML-5M spectrometer (fig 15). Both slit units are driven independently and can be positioned to record equal lengths of the same dispersed line or of different lines within the wavelength range of the instrument.

Position read out of the slit modules via a shaft encoder (coarse control) and three Moire graticule tracks (for fine control) gives an ultimate positional accuracy of better than 15 μm. At the time of writing the photoelectric scan unit, which will use channeltron detectors, has not been actively tested on a plasma. A comparably high resolution instrument with photographic emulsion and 2-channel photoelectric read out has been developed and used by Schwob [50].

We should not end our discussion on soft X-ray grating spectrometers without acknowledging the important developments in the technology of high efficiency laminar gratings and low light scatter holographicaly formed gratings [51]. For fusion studies we should like, ideally, to have true multi-channel spectral read-out. The use of toric substrates and holographicaly formed rulings can produce a nearly flat focal plane (at a preferred wavelength) and such an instrument, which might use a multi-element micro channel plate read-out system, has indeed been manufactured by Jobin-Yvon. A suite of gratings would be necessary for extended wavelength coverage; but it is not certain what the shortest wavelength limit of such an instrument might be. Such an instrument however, might well set the pattern for future grazing-incidence spectrometers.

We have mentioned the need in the spectroscopy of fusion plasmas for the calibration of the absolute incident photon flux against detector response. The absolute response of an instrument at characteristic K_α wavelengths can be measured with a gas flow proportional counter and an X-ray diode source with interchangeable anodes [52]; or from separate measurements of the diffraction grating efficiency and the detector response [53]. More conveniently in fusion experiments, the plasma itself often provides pairs of emission lines originating from a common upper level. If the emissivity of the plasma can be absolutely calibrated for one of the pair of lines, (this is generally feasible for the longer wavelength if it lies in the visible or VUV region, using a separate spectrometer of know light throughput) then the emissivity of the other line of the pair can be calculated. This branching ratio technique is commonly used [54] [55]. The use of MgF - windowed deuterium lamps as readiation transfer standards between 1150 Å [56] have proved particularly useful in the calibration of VUV spectrometers at the Culham laboratory. Branching ratio line pairs, belonging to He- and Li-like ions of light elements, which commonly appear in fusion devices and which the author has found particularly useful, are OVI, 150 Å/3811 Å; OVII 21.8 Å/1638.4 Å and CV 40.73 Å/2277.3 Å. Extension of the branching ratio pairs to shorter wavelength < 20 Å is possible using the iso-electronic transitions in fluorine and neon.

C. Crystal Spectrometers

Following our argument (section III A.(ii)) for a compact, spatially scanning crystal spectrometer the focusing Johann instrument illustrated in figure 18 has been designed and constructed. The four-pillar bending jig, see insert figure 18, holds an 8cm x 2cm crystal bent to a radius of curvature of 50cm. The spectrometer is designed to observe X-radiation in the range 0.5 to 25 Å from highly-ionised metals such as Ti Fe Mo and also from OVIII and OVII, these latter ions often being the most abundant ion species in tokamaks. The mean Bragg angle is altered by pivoting the Rowland circle about an axis through the crystal and orthogonal to the plane of dispersion. In order to view different chords through the plasma the whole vacuum assembly can be tilted.

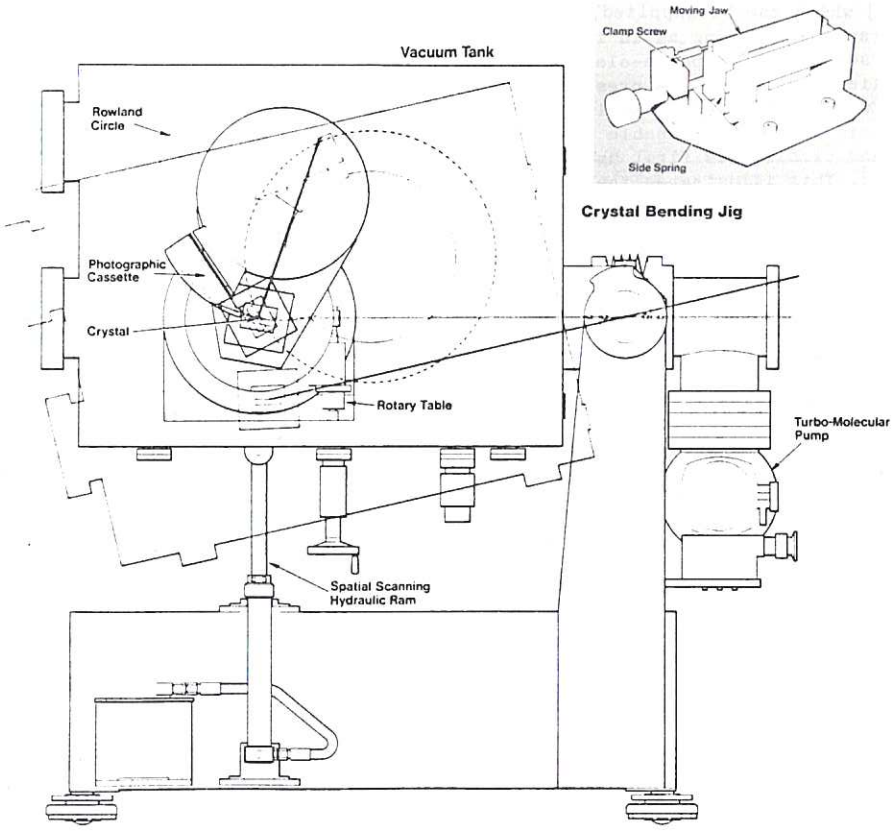

Fig 18. Optical layout of 0.5 m curved crystal spectrometer, using Johann mounting. The system is designed to observe dispersed radiation in the range 1 Å → 25 Å and can be plasma tilted to spatially scan a tokamak

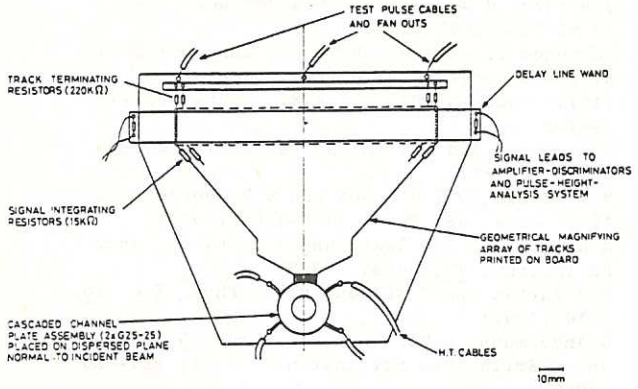

Fig 19. Schematic diagram of microchannel plate delay line readout assembly.

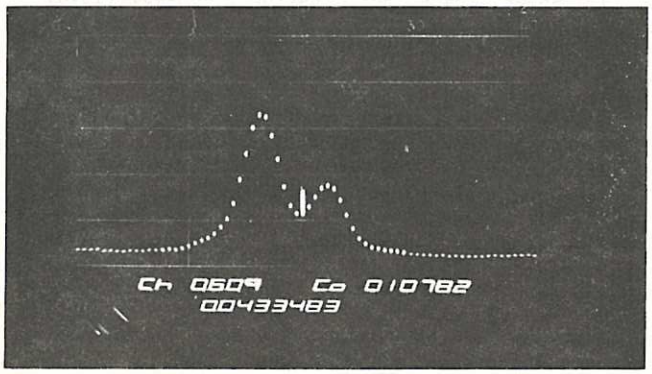

Fig 20. Resolution test of microchannel plate-delay line read out system shown in figure 19. The K_{α_1,α_2} lines from a Cn-anode X-ray tube is dispersed in 5th order by mica $\Delta\lambda(\alpha_1-\alpha_2)$ = 0.004 Å.

Alternative spectral read out systems are provided. In place of the photographic cassette, a multichannel electron multiplier plate (MCP) with a delay line read-out can be substituted, figure 19. Two cascaded micro-channel plates provide a gain of up to 10^8 and operate the delay line from a single photo-electron generated at the fron face of the MCP. A cloud of at least 10^6 electrons from the MCP is necessary to activate a signal from the delay line, the MCP and the delay line being connected electrically by a wand of conducting tracks. The wand, which is a printed circuit board, linearly expands the detector element frequency from 4/mm at the MCP to 4/cm at the delay line, the total number of resolving element in the latter being 1024. Tests indicate that the limitations to the MCP current density $\sim 10^5$ Hz per X-ray line and that the overall spatial resolution in the focal plane is $\sim$ 35μm [35]. In plasma experiments the plasma bandwidth recorded and the exposure time will be adjusted to the maximum count rate set by the electronics and to the access to a storage memory. Figure 20 shows a test spectrum of the $K_{\alpha_1\alpha_2}$ lines from Cu, dispersed in 5th order by a mica crystal. The separation between the α_1 and α_2 lines is 0.004 Å.

For the micron-size, transient high density plasmas, the above spectrometer is not at all appropriate. A de roglie instrument eg figure 12 has been extensively used for spectral surveys of laser-irradiated targets, see eg [57]. Without doubt however a space-resolving flat crystal instrument as in figure 13 is more appropriate when studying soft X-ray spectral features of laser-matter interactions.

ACKNOWLEDGEMENTS

The author would like to express his debt to the late M G Hobby, a resourceful collaborator in much of the X-ray instrument developments at the Culham laboratory. The paper has also benefited from discussions with J E Bateman, (the Rutherford laboratory), M F Stamp, (Oxford University), R K D Evans, (Leicester University) and R A Hulse (Princeton University).

REFERENCES

1. "Plasma Diagnostics and Data Acquisition Systems", Proc. of Course held by Int. School of Plasma Physics, Varenna, Italy (1975), A Eubank and E Sindoni editors, Milan: CNR-Euratom Plasma Physics Laboratory.
2. "Diagnostics for Fusion Experiments", Proc. of Course held by Int. School of Plasma Physics, Varenna, Italy (1978), E Sindoni and C Wharton editors. Published by Pergamon Press, Oxford (1979).
3. TFR Equipe, Nuclear Fusion, 18, 647-731 (1978).
4. D T Attwood, IEEE J, Quantum Electron 14, 909-923, (1978).
5. H G Ahlstrom, L W Coleman, F Rienecker and V W Slivinsky, J.Opt.Soc.Am, 68, 1731-1741, (1978).
6. N J Peacock and D D Burgess, Phil.Trans.Roy.Soc. London, A300, 665-682. (1981).
7. C DeMichelis and M Mattioli, Euratom-CEA Report (Fontenay-aux-Roses, France). EUR-CEA-FC-1084 (1981), to be published Nuc.Fus. (1981).
8. N M Ceglio and J T Larson, Phys.Rev.Letts 44, 579-582, (1980).
9. R M Gilgenbach et al, Phys.Rev.Letts, 44 No.10, 647-650, (1980).
10. TFR Group, "Heating in Toroidal Plasmas". Vol.2, 207-216. Joint Varenna-Grenoble Int. Symp. 1978. Published by Pergamon Press, (1979).
11. H Eubank, R J Goldston et al, Nucl.Fusion Suppl. 1, 167-197. Publ. IAEA Vienna (1979).
12. R E Chrien et al, Phys.Rev.Letts, 46, No.8, 535-538 (1981).
13. M Keilhacker, (IPP Garching, FDR), private communication on performance of ASDEX tokamak, (1981).
14. TFR Group, Plasma Physics 22, 851-860 (1980).
15. D E T F Ashby and M H Hughes - private communication, the Culham Laboratory (1981). Also R A Hulse, private communication, Princeton Plasma Physics Laboratory (1981).
16. N J Peacock, Culham Laboratory Report CLM-P619 (1980).
17. D E T F Ashby and M H Hughes, Culham Laboratory Report CLM-P625 (1980). See also contribution to 10th Euro. Conf on Controlled Fusion and Plasma Physics. Moscow, Sept. (1981).
18. M E Puiatti, R Breton, C De Michelis, and M Mattioli, Euratom-CEA Report, (Fontenay-aux-Roses). EUR-CEA-FC-1085 (1981).
19. N J Peacock and H P Summers, J.Phys.B. Atom. Molec.Phys., 11, No.21, 3757-3774, (1978).
20. K Brau, S Von Goeler, M Bitter, R D Cowan, D Eames, K Hill, N Sauthoff, E Silver, N Stodiek, Princeton Plasma Physics Laboratory Report, PPPL-1644 (1980)
21. A Salop, J.Phys.B:Atom.Molec.Phys., 12 No.6, 919-928 (1979).
22. R C Isler, Phys.Rev.Letts., 38, 1359-62, (1977).
23. R C Isler and L E Murray - see article by S Suckewer in Physica Scripta 23, No.2 72-86 (1981).
24. V V Afrosimov, S Yu Gordeev, A N Zinoviev and A A Korotkov. JETP Letts, 28, No.8 500-502 (1979).

25. N R Sauthoff, S Von Goeler and W Stodiek, Nucl. Fusion 18, 1445-1453 (1978).
26. J E Bateman and M G Hobby, Culham Laboratory Report, CLM-R204 (1980).
27. N J Peacock, Culham Laboratory Report, CLM-P626, (1980).
28. J D Kilkenny, R W Lee, M H Key and J G Lunney submitted to Phys.Rev. (1980).
29. B Yaakobi, D Steel et al, Phys.Rev. A19 1247-1262 (1977).
30. C C Smith and N J Peacock, J.Phys.B:Atom. Molec.Phys., 11,No, 15, 2749-2763, (1978).
31. D T Attwood, IEEE Jnl. of Quantum Electronics 14, No.12, 909-923, (1978).
32. A K Bhatia, U Feldman and G A Doschek, J.App. Phys., 51, 1464-80, (1980).
33. R J Groebner, N H Brooks and M Shimada, General Atomic Co. Report, GA-A16248 (1981).
34. G A Sawyer, A J Dearden, I Henins. F C Jahoda and F L Ribe, Phys.Rev. 131 1391-1397 (1963).
35. M G Hobby, N J Peacock and J E Bateman, Culham Laboratory Report, CLM-R203 (1980).
36. M Bitter, S Von Goeler, R Horton, M Goldman, K W Hill, N R Sauthoff and W Stodiek, Phys.Rev.Letts. 42 304-307 (1979).
37. P Platz, J Ramette, E Belin, C Bonnelle, A Gabriel, CEA-Euratom Report, (Fontenay-aux-Roses) EUR-CEA-FC-1057 (1980).
38. J P Pye, K D Evans et al, Astron. and Astrophys. 65, 123-138 (1978).
39. J E Mack, J R Stehn, B Edlen, J.Opt.Soc. Am. 22 245 (1932).
40. N J Peacock, "Laser Plasma Interactions" (Cairns and Sanderson, editors). Proc. of 20th Scottish Universities Summer School in Physics, pp 711-806 (1979).
41. Rutherford Laboratory - Annual Report to Laser Facility Committee. Report No. RL-79-036 (1979).
42. M H Key, C L S Lewis, J G Lunney, A Moore, J M Ward, R J Thareja, Phys.Rev.Lett. 44, No.25 1669-1672 (1980).
43. Lawrence Livermore Laboratory Annual Report of the Laser Programme. UCRL-50021-77 (1977), UCRL-50021-78 (1978), UCRL-50021-79 (1979).
44. N M Ceglio and H I Smith, Rev.Sc.Instr. 49 15-20 (1978).
45. N M Ceglio, D T Attwood and E V George, Jnl. Appl. Phys. 48, No.4, 1566-1569 (1977).
46. A H Gabriel, J R Swain and W A Waller, Jnl. Sc.Instrum. 42, 94-97 (1965)
47. W M Burton and R Wilson, Proc. Phys. Soc. 78, 1416 (1961).
48. G Andermann, L Bergknut, M Karras, G Grieshaber and J Smith, Rev.Sci.Instru, 51 (6), 814-820 (1980).
49. S Mrowka, private communication, Imperial College University of London, (1981).
50. TFR Group - J L Schwob. Euratom - CEA Report (Fontenay-aux-Roses). EUR-CEA-FC-1072 (1980).
51. R J Speer, Space. Sci. Instrum 2 463-487 (1976).
52. F J Morgan, A H Gabriel, M J Barton, J.Phys.E: Sci.Instrum. 1, 998-1002 (1966).
53. M G Hobby and N J Peacock, Jnl.Phys.E: Sci. Instrum. 6 854-857 (1973).
54. E Hinnov, "Diagnostics for Fusion Experiments" 139-148. Proc. Int. School of Plasma Physics, Association CNR-Euratom, Varenna, (Sindoni and Wharton, editors) publ. Pergamon Press, Oxford (1978).
55. F E Irons and N J Peacock, J.Phys.E:Sc. Instrum. 6, 857-862 (1973).
56. P J Key and R C Preston, J.Phys.E:Sci.Instrum. 13, 866-870 (1980).
57. H Gordon, M G Hobby and N J Peacock, J.Phys.B: Atom.Molec.Phys. 13, 1985-1999 (1980).